Asian Journal of Chemistry; Vol. 33, No. 4 (2021), 919-924

ASIAN JOURNAL OF CHEMISTRY

https://doi.org/10.14233/ajchem.2021.23097

Fabrication of Non-precious Vanadium Tungsten Nanocomposite for Enhanced Electrocatalytic Oxygen Reduction Reaction

L. Stanlykeninxavier[1,2], P. Elangovan[1,*] and M.S.S. Saravanakumaar[3,*]

[1]Department of Physics, Pachaiyappa's College, Chennai-600030, India
[2]Department of Physics, Government Girls Higher Secondary School, Thirumayam, Pudukkotai-622507, India
[3]Department of Physics, Saraswathi Narayanan College (Autonomous), Madurai-625022, India

*Corresponding authors: E-mail: drelangovanphysics@gmail.com; 2ssaravanakumar@gmail.com

Received: 12 December 2020; *Accepted*: 18 February 2021; *Published online*: 20 March 2021; AJC-20304

For the commercialization of alkaline fuel cells and metal air batteries, the advances in non-precious, cheap, stable electrocatalysts for the oxygen reduction reaction (ORR) and highly active remain a major problem. To overcome this problem, a facile approach was established to fabricate non-precious metal electrocatalysts, such as nanoparticles, pristine V_2O_5 and their WO_3 hybrids. This is the first study reporting the utilization of monoclinic-WO_3-nanocrystal-coupled V_2O_5 that serves as ORR catalysts. Compared with 50 wt.% WO_3 with 50 wt.% V_2O_5 (VW-2) spheres and pristine V_2O_5, the hybrid catalyst of 25 wt.% WO_3 and 75 wt.% V_2O_5 (VW-1) spheres exhibits outstanding catalytic activity towards ORR. In addition, the hybrid of 25 wt.% WO_3 and 75 wt.% V_2O_5 (VW-1) exhibits a higher long-term durability and catalytic activity than high-quality commercial Pt/C catalysts, which renders the composites of WO_3/V_2O_5 composites hybrid a high-capacity candidate for non-precious, high-performance, metal-based electrocatalysts having high efficiency and low cost for electrochemical energy conversion. The enhanced activity of WO_3/V_2O_5 composites is mainly obtained from the improved structural openness in the V_2O_5 tunnel structure when coupled with WO_3.

Keywords: Electrocatalysts, Oxygen reduction, Vanadium pentaoxide, Tungsten oxide, Fuel cells.

INTRODUCTION

In general, the electrocatalytic oxygen reduction reaction (ORR) is promoted through platinum catalyst and highly significant for the design of clean energy, such as fuel cells and metal-air batteries [1-8]. However, its commercial utilization is extremely limited by the high cost and scarceness of platinum. Numerous studies [1,9-11] have focused on low-cost ORR catalysts for replacing the expensive Pt-based catalyst. Similar to platinum catalysts, metal-doped carbon catalysts fabricated by employing the pyrolysis of a combination of nitrogen/carbon based precursors and transition metal salts show high ORR activities [12]. As efficient ORR catalysts, heterostructured composites have recently attracted considerable attention. Various catalysts have been prepared with and without carbon [1,4,13-18].

Notably, the development and rapid progress of vanadium and/or tungsten centered catalysts deliver abundant openings to possibly resolve the catalytic activity and durability concerns for ORR [10,19-22]. Typically, the ORR activity and the long term durability significantly depend on the catalytic active sites of the exposed surface and the high-surface-to-volume ratios, sintering and decomposition as well as the dimension impart of the catalysts. In addition, commercial V_2O_5-WO_3/TiO_2 catalysts have a short operating life due to the instability of the active components and high-temperature sintering [23]. Thus, it is urgently desirable to develop an efficient and green way to produce highly efficient catalysts with long term durability.

In this study, an efficient heterostructured catalysts based on WO_3 and V_2O_5 is developed. Herein, the synthesis and electrocatalytic properties of highly active catalyst prepared by a solution assisted annealing method. Indeed, the specific highly ordered 25 wt.% WO_3-loaded V_2O_5 catalyst exhibits superior activity as compared to pure V_2O_5 with long term durability.

EXPERIMENTAL

All chemical reagents like ethanol (> 99.5%), ammonium metavanadate (NH_4VO_3, > 99%) and 12-phosphotungstic acid ($H_3PW_{12}O_{40}$, > 98%) were acquired from Sigma-Aldrich, USA. Classically, the synthesis method was slightly modified with the reported template assisted method [24]. In a typical preparation, required amount of NH_4VO_3 was dispersed on ethanol solution, the mixture was vigorously stirred for 3 h at room temperature and the acquired solid was quarantined by filtration and dried at 100 ºC for 12 h. Then, certain amounts of the dried product and 12-phosphotungstic acid (PTA) were added in 50 mL of absolute ethanol and the resulting mixture was stirred at room temperature until complete evaporation of the solvent (~ 48 h) took place. The dry powder was heated to 550 ºC (1 ºC per min ramping rate) for 5 h to decompose NH_4VO_3 and 12-phosphotungstic acid (PTA) to yield highly ordered V_2O_5/WO_3 composite. The amount of WO_3 and NH_4VO_3 used in reactions varied between 0.025, 0.050 M, 0.075 and 0.05 M to gives a series of V_2O_5/WO_3 composites with different loading amount of WO_3. The varied amount of 0.025 M and 0.050 M WO_3 were assorted with varied amount of 0.075 M and 0.050 M NH_4VO_3 to gives a series of V_2O_5/WO_3 composites with different loading amount of WO_3. For easy understanding, the catalysts prepared using 0.025 M and 0.050 M WO_3 with varied amount of 0.075 M and 0.050 M NH_4VO_3 samples were named as VW-1 and VW-2, respectively. Similarly, vanadium oxide composite (V_2O_5) was also prepared following a similar procedure without using WO_3.

Characterization: The crystalline phases of the prepared samples were examined using X-ray diffraction (XRD) analysis (Bruker AXS D8, Bruker, Germany). The surface morphology of the samples was examined by field-emission scanning electron microscopy (FE-SEM; JSM 6500F). The concentrations of elements in each solution were analyzed using an inductively coupled plasma-optical emission spectrometer (ICP-OES, Optima 8000, Perkin-Elmer, Shelton, CT 06484, USA). The chemical composition and elements present in samples and their corresponding valence states in samples were determined by X-ray photoelectron spectroscopy (XPS). The measurements were acquired by an ESCALab220i-XL electron spectrometer (Thermo-Fisher Scientific Company, USA). The vibrational, rotational and other low-frequency modes in the sample were analyzed by Raman spectroscopy (Thermo-Scientific DXR).

Electrochemical measurements: All electrochemical measurements were conducted at room temperature in 0.1 M KOH through cyclic voltammetry by using a rotating disk electrode. The three-electrode cell comprised Ag/AgCl, Pt, a glass carbon/rotating disk (loaded with various catalysts) electrodes as the reference, counter and working electrodes, respectively. For the working electrode, in 10 mL of Nafion solution (0.5 wt% in isopropanol) and ethanol (1 mg mL^{-1}), electroactive composite were mixed as a binder through sonication. Afterwards, on glassy carbon RDEs, catalysts with approximately 0.10 mg cm^{-2} of binder were coated. For electrochemical characterizations, these catalysts were dried in air. Finally, by using the Nernst equation, Ag/AgCl versus the measured potential was converted into a reversible hydrogen electrode (RHE) scale [25-27].

RESULTS AND DISCUSSION

The crystalline structure and chemical nature of the prepared products were characterized using XRD, XPS and Raman spectroscopy. Fig. 1 shows the X-ray diffraction patterns of pure V_2O_5, VW-1 and VW-2 nanoparticles. In bare V_2O_5, all diffraction peaks could be certainly indexed to the orthorhombic phases (JCPDS card No. 41-1426 orthorhombic V_2O_5. However, WO_3 doped V_2O_5 samples display a mixture of a major monoclinic pattern (JCPDS card no. 043-1035) with orthorhombic phases (JCPDS Card No. 41-1426 orthorhombic V_2O_5) in the XRD pattern. For the strongest peak, with an increase in the WO_3 dopant concentration, the full width at half maximum (FWHM) increases and the intensity decreases. Furthermore, these peaks shift towards the lower angle compared with the peaks of pristine V_2O_5 because the ionic radii of V^{4+}, V^{5+} and V^{3+} ions are similar to those of the W^{6+} ion. The XPS revealed multiple valences (Fig. 2). In tungsten crystal sites, small vanadium

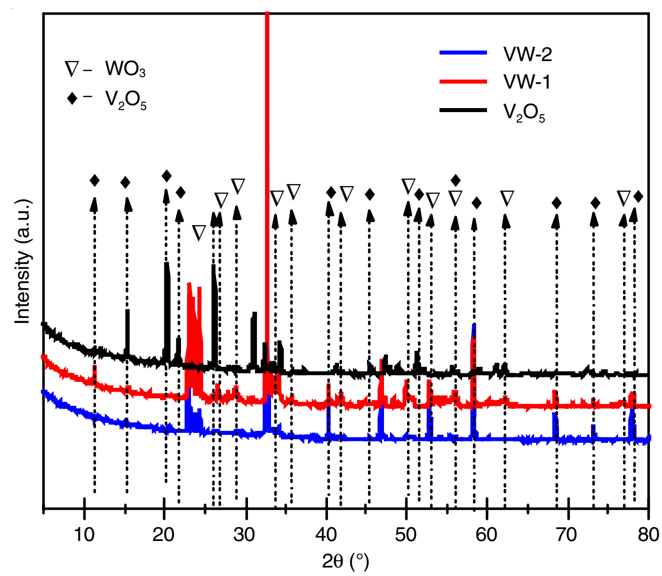

Fig. 1. XRD patterns of prepared samples

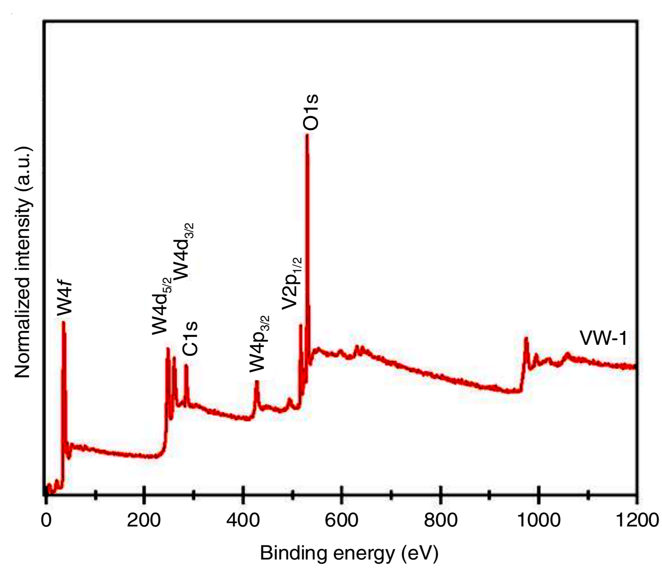

Fig. 2. XPS spectra of VW-1 catalyst

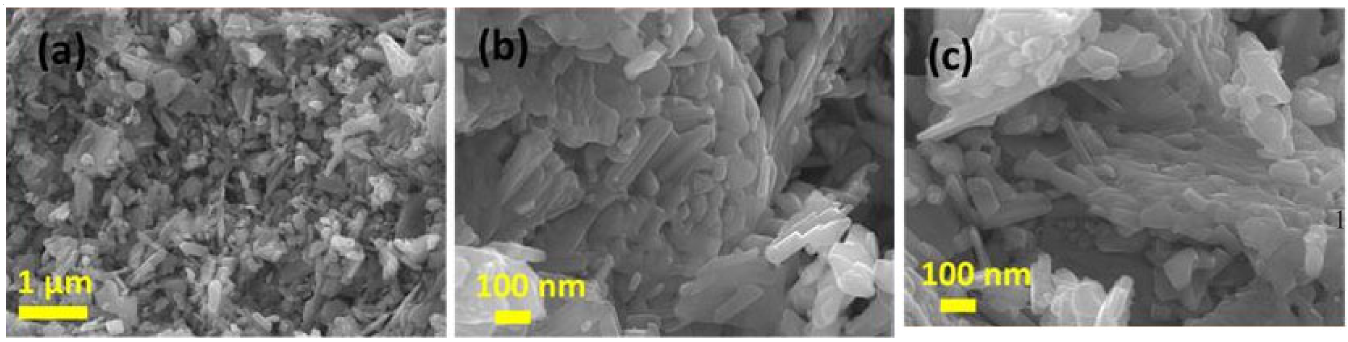

Fig. 3. Field-emission scanning electron microscopic images of bare V_2O_5

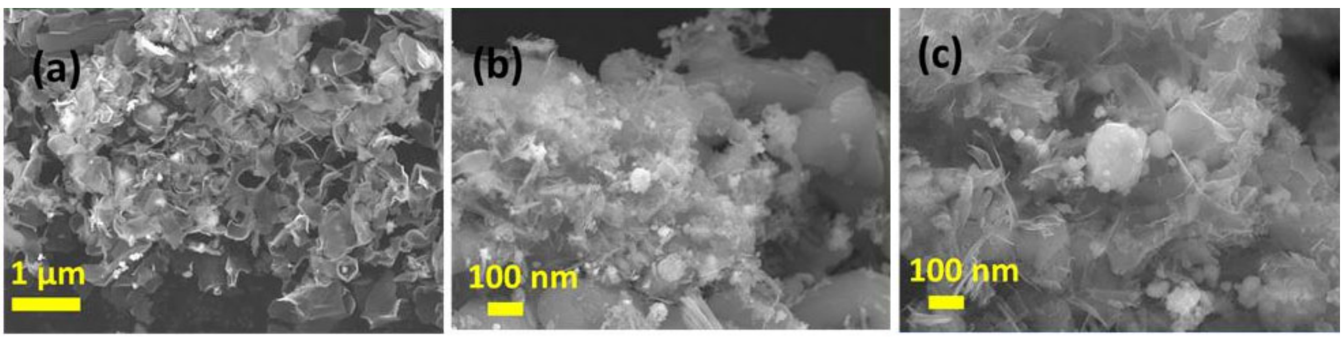

Fig. 4. Field-emission scanning electron microscopic images of VW-1

ions can easily enter, which might lead to an ordered system and a lower diffraction angle and higher FWHM. This result is in strong agreement with Raman and XPS analyses. A small WO_3 doping amount can efficiently tune the V_2O_5 electronic nature.

When the doping concentration is adequately high, dopants likely annihilate the semiconducting nature of hosts. Further, dopant of WO_3 concentrations on VW-1 and VW- 2 samples were accurately identified as 24.6 wt.% and 50.1 wt.%, respectively. Two sharp peaks with binding energies at 35.63 and 37.71 eV can be observed (Fig. 2), which are related with the characteristic $4f_{7/2}$ and $4f_{5/2}$ peaks of the W^{6+} species, indicate the co-existence of W^{5+} ions with oxygen vacancies, the elemental composition of tungsten is about 8 %. In addition, different peak areas of W^{5+} show that the VW-1 nanoparticles possess considerable oxygen vacancies. The elemental composition of 19 % vanadium and 73% oxygen indicates an almost ideal stoichiometry of the single crystals with all vanadium present as V^{5+} species. That fact is also reflected by characteristic V^{5+} positions of V2*p* and O1*s* photoemission lines located at 517.1 and 531.6 eV.

The size, morphology and hybrid structure of all the samples were examined by scanning electron microscopy. Fig. 3 shows the microscopic images of pristine V_2O_5 nanoflakes. The microscopic images (Figs. 4 and 5) of the prepared WO_3/V_2O_5 samples evidently show a unique mesoporous nanosheets like morphology, where the average width of the hybrid is found to be 100-125 nm. Besides, it is to be noted that V_2O_5 nanoflakes with an average diameter of ~20-40 nm were obtained. In general, during syntheses, organic additives play an important role in directing crystal growth and inducing WO_3/V_2O_5 nanoflake nuclei. For controlling the nanostructure morphology,

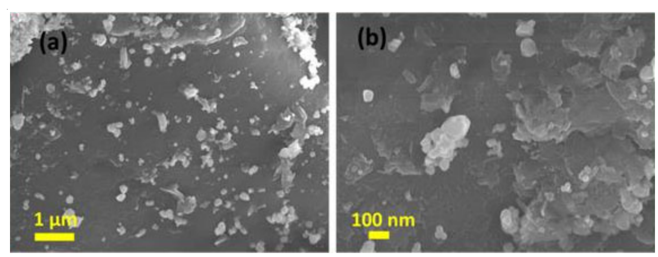

Fig. 5. Field-emission scanning electron microscopic images of VW-2

the effect of ammonium ions on growth and nucleation is critical. Furthermore, crystallization with a flake-like shape occurs for H_2O and NH^{4+}. Finally, the crystallinity and purity of the samples were improved using the temperature effect.

For electro-catalytic applications, to obtain the most suitable catalyst, comparative cyclic voltammetry (CV) was studied at a scan rate of 10 mV s^{-1} in O_2 and Ar saturated 0.1 M KOH by using the three-electrode system to determine the ORR performance of the fabricated samples (Fig. 6). In contrast to Ar, for bare V_2O_5, a distinct characteristic ORR peak, which was centred at 0.56 V *versus* RHE and having a 0.28 mA cm^{-2} reaction current density, was observed when O_2 was hosted. From the rotating ring disk electrode, a higher and lower ORR reaction current and onset potential, respectively, indicated a more effortless ORR process for this catalyst (Fig. 6). For the study of CV behaviour, in an argon (Ar)-saturated or oxygen (O_2)-saturated 0.1 M KOH electrolyte at the potential scan rate of 10 mV s^{-1}, re-producible CVs were acquired by using the three-electrode technique to evaluate the activity of electrochemical oxygen reduction. For this assessment, a high-quality commercial PtC (HiSPEC™ 4000, Johnson Matthey, 10 wt.% Pt), the fabricated WO_3/V_2O_5 composites and V_2O_5, having the same loadings were loaded onto the glassy carbon electrode. In the Ar-saturated electrolyte, the discreet CV profile was observed (dotted block line, Fig. 6). In an O_2-saturated electrolyte, a robust reduction peak current was observed (solid red line, Fig. 6). This finding revealed a high electro-catalytic activity for cathodic oxygen reduction by WO_3/V_2O_5 composites. The WO_3/V_2O_5 composite (VW-1) exhibited an ORR peak shift towards the negative potential compared with VW-2 and bare V_2O_5. To understand the reaction kinetics and electrocatalytic activity of all the catalysts fabricated using the highly pure commercial Pt/C sample and WO_3/V_2O_5 towards ORR, the linear sweep voltammogram of polarization curves were acquired using the rotating disk electrode in the O_2-saturated 0.1 M KOH electrolyte at different rotation rates and the scan rate of 10 mV s^{-1} (Fig. 6). Additionally, the wide and unique current plateau of 0.1-1.0 V *versus* RHE obtained for the entire electrode indicated the diffusion-controlled process, which corresponded to an efficient ORR pathway for 2.7-3.12 electron transfer. This finding is in a strong agreement with metal oxide electrocatalysts reported in literature for ORR [28-30]. Furthermore, at other potentials, the Koutecky-Levich (K-L) plots were obtained (Fig. 6). For all the fabricated catalysts, the plots exhibited good linearity. At dissimilar potentials, these plots indicated related electron transfer numbers for ORR and the first-order kinetic reaction towards the dissolved oxygen concentration. For VW-1, the higher and steadier electron-transfer numbers revealed a more electrochemically stable and smoother ORR activity.

Fig. 6a illustrates the polarization curves for ORR acquired on a the rotating disk electrode at 1600 rpm by using WO_3/V_2O_5 composites, V_2O_5 and commercial 10 wt.% Pt/C catalysts in the O_2-saturated 0.1 M KOH solution. Sample VW-1 exhibited a considerably high ORR onset potential of 0.796 V *versus* RHE, which was close to that of commercial 10 wt.% Pt/C (0.972 V *vs.* RHE) and substantially more positive than that of VW-2 (0.651 V *vs.* RHE) and V_2O_5 (0.638 vs. RHE), at 1600 rpm. At 0.6 V *vs.* RHE, the VW-1, V_2O_5 and VW-2 catalysts showed the ORR activity with the electron transfer number of 3.12, 2.73 and 3.1, respectively (Fig. 6). Compared with the fabricated catalysts, WO_3/V_2O_5 (VW-1) exhibited improved ORR performance because the high metallic nature, optimal concentration, smooth surface morphology, exposed active faces, large surface area and mesoporous nature of WO_3 have significant effects on the catalytic activities of VW-1. During

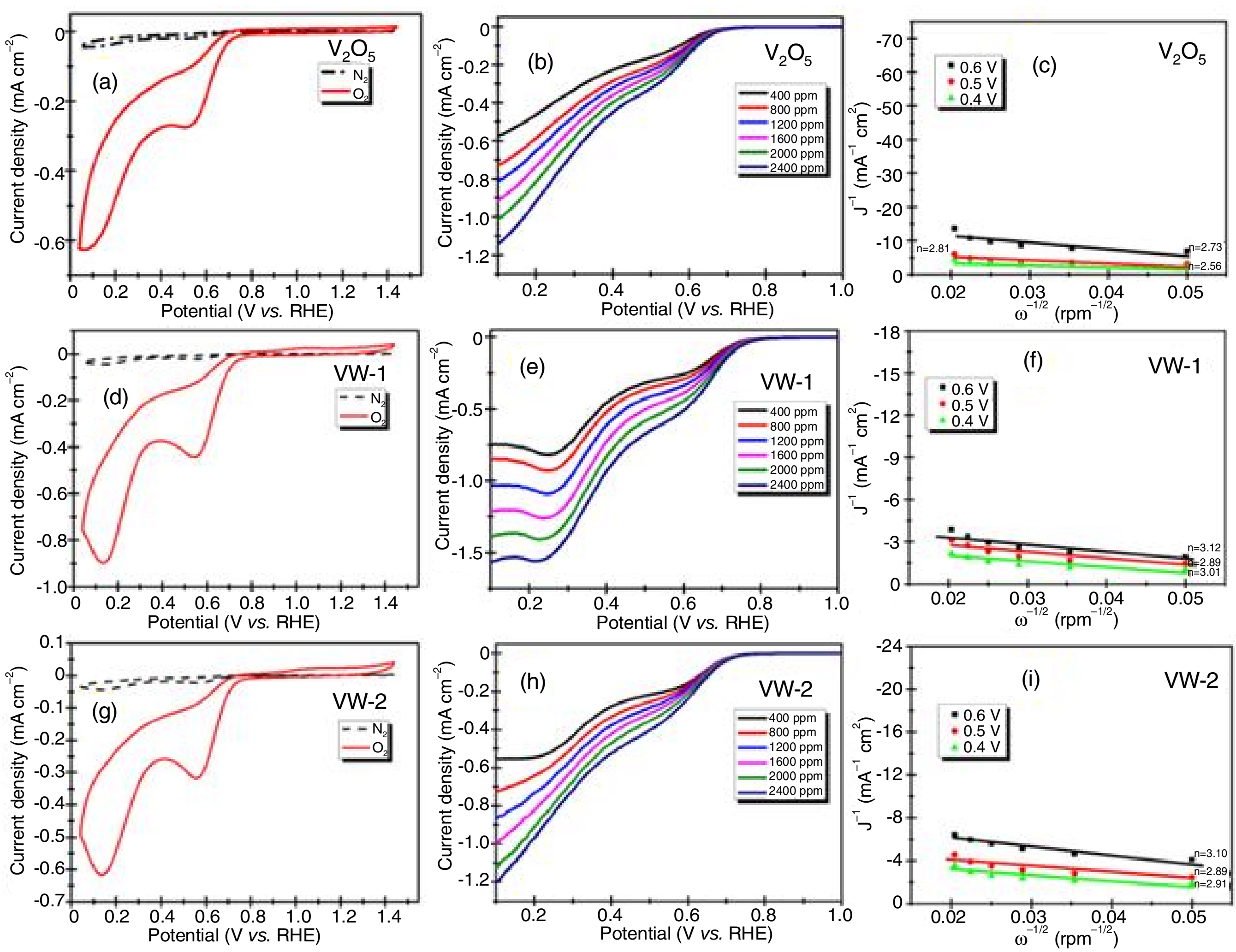

Fig. 6. Electrocatalytic performance of prepared samples, (a-c), (d-f) and (g-i) are cyclic voltammetry and linear sweep voltammetry curves and K-L plots for V_2O_5, VW-1 and VW-2 catalysts respectively, in 0.1 M KOH at a sweep rate of 10 mV s^{-1}

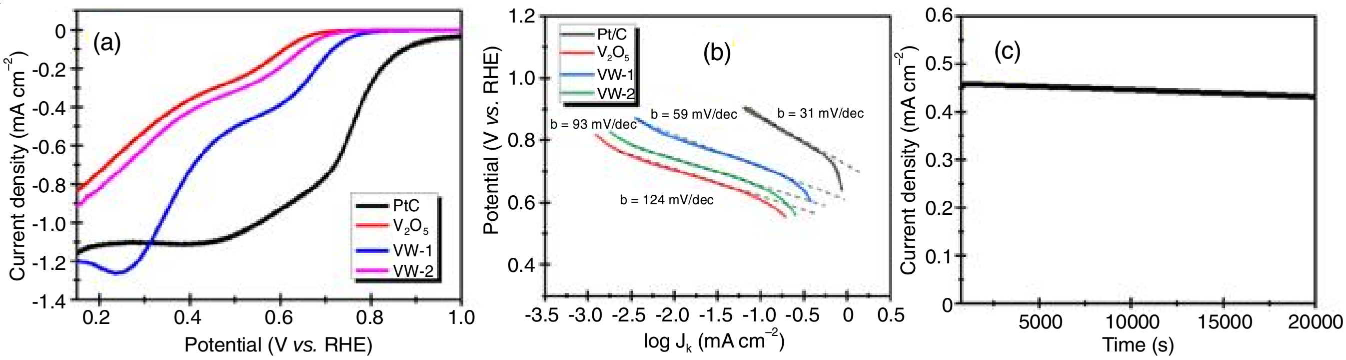

Fig. 7. LSV polarization curves for the ORR obtained with WO_3, V_2O_5/WO_3 composites, and commercial 10 wt. % PtC catalysts on a rotating disk electrode (RDE) in an O_2-saturated 0.1 M KOH solution at 1600 rpm (b) corresponding Tafel plot and (c) long term durability test under 0.1 M KOH at a fixed potential of 0.65 V *vs.* RHE

syntheses, nanoparticles with a narrow band gap are used because their high-conduction band edge position is beneficial for catalytic reactions.

Moreover, at 0.2 V *vs.* RHE, the V_2O_5, VW-1 and VW-2 catalysts exhibited an ORR current density of -0.79 mA cm^{-2}, -1.23 mA cm^{-2} and -0.85 mA cm^{-2}, respectively (Fig. 7). Compared to other catalysts, the ORR performance of WV-1 catalyst was enhanced greatly. With increasing amount of WO_3, the VW-1catalyst showed poorer performance. This may be due to the high degree of aggregation and low contact area between the WO_3 and V_2O_5 catalysts. In addition, the ORR current at 0.1 V *vs.* RHE of the VW-1 was slightly higher than that of a commercial Pt/C catalyst and the half-wave potential was ~ 232 mV lower than that of Pt/C. The higher ORR activity of the VW-1 catalyst was also observed from the much smaller Tafel slope of ~ 59 mV/decade at low over-potentials (Fig. 7) compared to those measured using V_2O_5 (~ 124 mV/decade), VW-2 (~ 93 mV/decade) and high quality commercial Pt/C, which showed ~ 31 mV/decade in the O_2 saturated 0.1M KOH electrolyte, suggesting promising ORR reaction kinetics in the VW-1 electrocatalyst.

In addition to high ORR activity, the long-term durability of electrocatalysts is crucial because it is used to govern the cycle life of metal-air batteries and fuel cells. For VW-1, a 20,000-s chronoamperometric (i-t) test was performed at –0.65 V *versus* RHE with a high rotation speed (1600 rpm). VW-1 exhibited excellent performance (∇ 4.51 mA cm^{-2}) (Fig. 7c). Almost no cathodic current attenuation was observed (less decay, approximately ∇ 0. 21 mA cm^{-2}). This result indicated that WO_3/V_2O_5 presents a good long-term durability. This long-term durability is particularly beneficial to alkaline fuel cells.

Conclusion

This article reported a new type of metal oxide composites electrocatalyst for the oxygen reduction reaction (ORR). The excellent catalysts composed of an ordered, WO_3 and V_2O_5. Outstanding electrocatalytic performance toward oxygen reduction under alkaline medium is achieved by selecting a highly active and optimum concentration of WO_3 on WO_3/V_2O_5 composite. The outstanding catalytic activity of 75 wt.% V_2O_5 (VW-1) with 25 wt.% WO_3 catalyst for ORR was attributed to the optimum concentration, high conductivity, high surface area and mesoporous nature of WO_3 because these properties help in reducing the overpotential, in facilitating electrochemical activity and in reducing Tafel values to less than those values of other catalysts. Additionally, this catalyst has long-term durability. An optimal amount of WO_3 leads to control over the geometric, structural, electronic effects and provides smooth surface morphology. A definite composition, large surface area and structure are energetically advantageous for the catalyst durability and ORR. This study proposed a new design approach for the synthesis of highly potential catalysts having multiple benefits for metal-air batteries, next-generation alkaline fuel-cell catalysts, drug delivery, photonic devices, heterogeneous catalysis and photo catalysis with a long-term durability and an outstanding activity.

CONFLICT OF INTEREST

The authors declare that there is no conflict of interests regarding the publication of this article.

REFERENCES

1. Z. Chen, D. Higgins, A. Yu, L. Zhang and J. Zhang, *Energy Environ. Sci.*, **4**, 3167 (2011); https://doi.org/10.1039/c0ee00558d
2. S. Chandrasekaran and S.H. Hur, *Mater. Res. Bull.*, **112**, 95 (2019); https://doi.org/10.1016/j.materresbull.2018.12.010
3. S. Chandrasekaran, E.J. Kim, J.S. Chung, C.R. Bowen, B. Rajagopalan, V. Adamaki, R. Misra and S.H. Hur, *J. Mater. Chem. A Mater. Energy Sustain.*, **4**, 13271 (2016); https://doi.org/10.1039/C6TA05043C
4. M. Khandelwal, S. Chandrasekaran, S.H. Hur and J.S. Chung, *J. Power Sources*, **407**, 70 (2018); https://doi.org/10.1016/j.jpowsour.2018.10.055
5. M. Liu, Z. Zhao, X. Duan and Y. Huang, *Adv. Mater.*, **31**, 1802234 (2019); https://doi.org/10.1002/adma.201802234
6. S. Chandrasekaran, D. Ma, Y. Ge, L. Deng, C. Bowen, J. Roscow, Y. Zhang, Z. Lin, R.D.K. Misra, J. Li, P. Zhang and H. Zhang, *Nano Energy*, **77**, 105080 (2020); https://doi.org/10.1016/j.nanoen.2020.105080
7. S. Chandrasekaran, C. Bowen, J. Roscow, Y. Zhang, D.K. Dang, E.J. Kim, R.D.K. Misra, L. Deng, J.S. Chung and S.H. Hur, *Phys. Rep.*, **792**, 1 (2019); https://doi.org/10.1016/j.physrep.2018.11.001
8. W. Liu, P. Geng, S. Li, R. Zhu, W. Liu, H. Lu, S. Chandrasekaran, Y. Pang, D. Fan and Y. Liu, *Int. J. Hydrogen Energy*, **45**, 28576 (2020); https://doi.org/10.1016/j.ijhydene.2020.07.144

9. H.T. Chung, D.A. Cullen, D. Higgins, B.T. Sneed, E.F. Holby, K.L. More and P. Zelenay, *Science*, **357**, 479 (2017); https://doi.org/10.1126/science.aan2255
10. A. Elmouwahidi, E. Bailón-García, A.F. Pérez-Cadenas, J. Castelo-Quibén and F. Carrasco-Marín, *Carbon*, **144**, 289 (2019); https://doi.org/10.1016/j.carbon.2018.12.038
11. S. Chen, S. Chandrasekaran, S. Cui and X. Zhang, *Inorg. Chem. Commun.*, **120**, 108159 (2020); https://doi.org/10.1016/j.inoche.2020.108159
12. J. Zhu, J. Roscow, S. Chandrasekaran, L. Deng, P. Zhang, T. He, K. Wang and L. Huang, *ChemSusChem*, **13**, 1275 (2020); https://doi.org/10.1002/cssc.201902685
13. J. Kim, H.E. Kim and H. Lee, *ChemSusChem*, **11**, 104 (2018); https://doi.org/10.1002/cssc.201701306
14. V. Kashyap, S.K. Singh and S. Kurungot, *ACS Appl. Mater. Interfaces*, **8**, 20730 (2016); https://doi.org/10.1021/acsami.6b05416
15. A. Kumar, Y. Zhang, W. Liu and X. Sun, *Coord. Chem. Rev.*, **402**, 213047 (2020); https://doi.org/10.1016/j.ccr.2019.213047
16. Q. Lv, N. Wang, W. Si, Z. Hou, X. Li, X. Wang, F. Zhao, Z. Yang, Y. Zhang and C. Huang, *Appl. Catal. B*, **261**, 118234 (2020); https://doi.org/10.1016/j.apcatb.2019.118234
17. J. Liang, Y. Jiao, M. Jaroniec and S.Z. Qiao, *Angew. Chem. Int. Ed.*, **51**, 11496 (2012); https://doi.org/10.1002/anie.201206720
18. M. Song, Y. Song, W. Sha, B. Xu, J. Guo and Y. Wu, *Catalysts*, **10**, 141 (2020); https://doi.org/10.3390/catal10010141
19. J. Li, S. Huang, G. Zhang, Z. Li, S. Tong, J. Wang and M. Wu, *Chem. Commun.*, **56**, 1823 (2020); https://doi.org/10.1039/C9CC08980B
20. S. Chandrasekaran, P. Zhang, F. Peng, C. Bowen, J. Huo and L. Deng, *J. Mater. Chem. A Mater. Energy Sustain.*, **7**, 6161 (2019); https://doi.org/10.1039/C8TA12238E
21. K. Maiti, J. Balamurugan, J. Gautam, N.H. Kim and J.H. Lee, *ACS Appl. Mater. Interfaces*, **10**, 32220 (2018); https://doi.org/10.1021/acsami.8b11406
22. I.A. Rutkowska, A. Wadas, S. Zoladek, M. Skunik-Nuckowska, K. Miecznikowski, E. Negro, V.D. Noto, A. Zlotorowicz, P. Zelenay and P.J. Kulesza, *J. Electrochem. Soc.*, **165**, J3384 (2018); https://doi.org/10.1149/2.0491815jes
23. J.-K. Lai and I.E. Wachs, *ACS Catal.*, **8**, 6537 (2018); https://doi.org/10.1021/acscatal.8b01357
24. E. Skliri, I.N. Lykakis and G.S. Armatas, *RSC Adv.*, **4**, 46170 (2014); https://doi.org/10.1039/C4RA07850K
25. S. Chandrasekaran, J.S. Chung, E.J. Kim and S.H. Hur, *Chem. Eng. J.*, **290**, 465 (2016); https://doi.org/10.1016/j.cej.2016.01.029
26. S. Chandrasekaran, E.J. Kim, J.S. Chung, I.-K. Yoo, V. Senthilkumar, Y.S. Kim, C.R. Bowen, V. Adamaki and S. Hyun Hur, *Chem. Eng. J.*, **309**, 682 (2017); https://doi.org/10.1016/j.cej.2016.10.087
27. S. Chandrasekaran, L. Yao, L. Deng, C. Bowen, Y. Zhang, S. Chen, Z. Lin, F. Peng and P. Zhang, *Chem. Soc. Rev.*, **48**, 4178 (2019); https://doi.org/10.1039/C8CS00664D
28. H.-Y. Su, Y. Gorlin, I.C. Man, F. Calle-Vallejo, J.K. Nørskov, T.F. Jaramillo and J. Rossmeisl, *Phys. Chem. Chem. Phys.*, **14**, 14010 (2012); https://doi.org/10.1039/c2cp40841d
29. C. Goswami, K.K. Hazarika and P. Bharali, *Mater. Sci. Energy Technol.*, **1**, 117 (2018); https://doi.org/10.1016/j.mset.2018.06.005
30. H. Osgood, S.V. Devaguptapu, H. Xu, J. Cho and G. Wu, *Nano Today*, **11**, 601 (2016); https://doi.org/10.1016/j.nantod.2016.09.001